Independent Control of the Magnetization in Ferromagnetic $La_{2/3}Sr_{1/3}MnO_3/SrTiO_3/LaCoO_3$ Heterostructures Achieved by Epitaxial Lattice Mismatch

Beatriz Rivas-Murias,[†] Irene Lucas,[‡,§] Pilar Jiménez-Cavero,[‡,§] César Magén,[§,∥,⊥] Luis Morellón,[‡,§] and Francisco Rivadulla*[,†]

[†]Centro de Investigación en Química Biológica y Materiales Moleculares (CIQUS), Universidad de Santiago de Compostela, 15782 Santiago de Compostela, Spain

[‡]Instituto de Nanociencia de Aragón (INA), Universidad de Zaragoza, Mariano Esquillor, Edificio I+D, 50018 Zaragoza, Spain

[§]Departamento Física de la Materia Condensada, Universidad de Zaragoza, Pedro Cerbuna 12, 50009 Zaragoza, Spain

[∥]Laboratorio de Microscopías Avanzadas (LMA), Instituto de Nanociencia de Aragón (INA), Mariano Esquillor, Edificio I+D, 50018 Zaragoza, Spain

[⊥]Fundación ARAID, 50018 Zaragoza, Spain

ABSTRACT: We report the effect of interface symmetry-mismatch on the magnetic properties of $LaCoO_3$ (LCO) thin films. Growing epitaxial LCO under tensile strain on top of cubic $SrTiO_3$ (STO) produces a contraction along the *c* axis and a characteristic ferromagnetic response. However, we report here that ferromagnetism in LCO is completely suppressed when grown on top of a buffer layer of rhombohedral $La_{2/3}Sr_{1/3}MnO_3$ (LSMO), in spite of identical in-plane and out-of-plane lattice deformation. This confirms that it is the lattice symmetry mismatch and not just the total strain, which determines the magnetism of LCO. On the basis of this control over the magnetic properties of LCO, we designed a multilayered structure to achieve independent rotation of the magnetization in ferromagnetic insulating LCO and half-metallic ferromagnet LSMO. This is an important step forward for the design of spin-filtering tunnel barriers based on LCO.

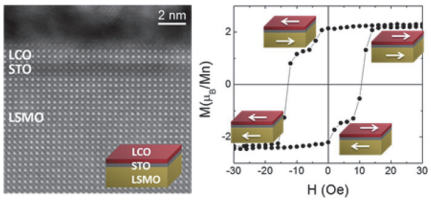

KEYWORDS: *$LaCoO_3$, ferromagnetic-insulator, spin-filter tunnel junction, thin-film, epitaxial multilayers, exchange-bias*

Ferromagnetic insulating (FMI) oxides have important applications in the design of multiferroic materials and fabrication of spin-filter tunnel barriers in spintronic applications.[1] The utility of FMI tunnel barriers was demonstrated by Moodera et al.[2−5] with EuS, and it was later shown in other oxides like $La_{0.1}Bi_{0.9}MnO_3$,[6,7] $Pr_{0.8}Ca_{0.2}Mn_{1-x}Co_xO_3$,[8] $NiFe_2O_4$,[9,10] and $CoFe_2O_4$.[10−14] In these cases, the fundamental magnetic interaction is antiferromagnetic (AF), nevertheless giving rise to ferromagnetism (FM) as a result of uncompensated magnetic moments (as in ferrimagnetic spinels), or canted AF (in the perovskites). But unfortunately, apart from a few notable exceptions, FM oxides tend to be conducting.[15] Therefore, the synthesis of new FMI oxides is an important and interesting challenge that must be addressed.

In this regard, the FMI state induced by epitaxial strain in $LaCoO_3$ (LCO) thin films is remarkable.[16−20] Given the similarities between the intra-atomic exchange and the crystal field splitting of Co^{3+} in LCO (≈20−80 meV),[21,22] some authors associated the FM in thin films of LCO to an ordered pattern of HS/LS Co^{3+} stabilized by strain.[23−25] However, oxygen nonstoichiometry was also suggested by other authors as the main responsibility of FM,[26−28] and the precise origin of this effect is still under debate. Recently, Qiao et al.[29] proposed a correlation between the macroscopic magnetism observed in films of LCO under tensile stress and the microscopic octahedral distortions induced by the symmetry mismatch at the interface. These authors suggest that an octahedral expansion induced by epitaxial stress reduces the Co−O bond covalency and promote higher spin states of Co^{3+}, which supports the FM interaction.

In this work, we explored the magnetic behavior of LCO grown on a buffer layer of half-metallic FM $La_{2/3}Sr_{1/3}MnO_3$ (LSMO) over STO. Bulk LSMO crystallizes in a rhombohedral structure ($R\bar{3}c$, number 167) like LCO, and both show similar out-of-phase octahedral rotation in the three directions of space ($a^-a^-a^-$ in Glazer notation[30]). This experiment is, therefore, a macroscopic test for the microscopic theory of FM in LCO induced by symmetry mismatch with STO. Our results confirmed a complete suppression of FM in LCO grown on top of a buffer layer of LSMO on STO, in spite of a lattice deformation identical to that achieved by direct growth on

STO. On the basis of this precise control over the FM of LCO, we designed a multilayered structure in which the magnetization of FMI LCO and FMM LSMO can be manipulated independently. This is an important first step to develop FMI barriers of LCO for application in spin-filter tunnel devices.

Results and Discussion. Different multilayered structures of LCO and LSMO were grown by pulsed laser deposition (PLD) on (001)-oriented STO substrates:

(i) Two bilayers (all units in nanometers): LSMO(22)-bottom/LCO(4)-top (hereafter LSMO/LCO) and LCO(4)-bottom/LSMO(22)-top (hereafter LCO/LSMO).

(ii) Two trilayers (all units in nanometers): LCO(4)-bottom/LSMO(20)-middle/LCO(4)-top (hereafter LCO/LSMO/LCO) and LSMO(22)-bottom/STO(1)-middle/LCO(2)-top (hereafter LSMO/STO/LCO).

X-ray diffraction and reflectivity, as well as aberration corrected scanning transmission electron microscopy (STEM), indicate the growth of coherently strained epitaxial layers, with atomically sharp and flat interfaces over large distances (see for example X-ray reciprocal space maps in Figure S2 in the Supporting Information and Figures 1 and 2 below), certifying the high-quality of the samples in this study.

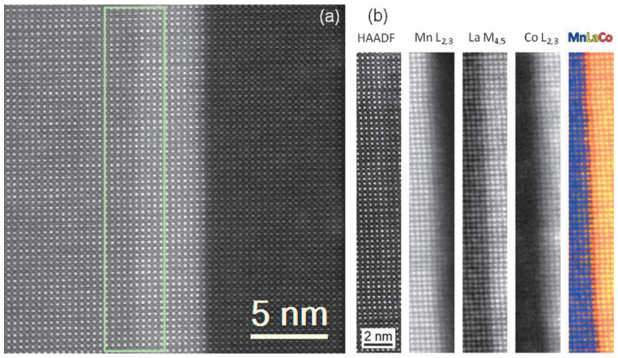

Figure 1. STEM-EELS spectrum image of the LSMO-LCO interface collected in the region of interest, marked with a green rectangle in the HAADF reference image (a). (b) Panels show the HAADF signal; Mn $L_{2,3}$, La $M_{4,5}$, and Co $L_{2,3}$ integrated intensities, and color map composed with these intensity distributions.

Epitaxial growth on (001) STO imposes a tensile stress of +0.62% and +2% on LSMO and LCO, respectively. In a purely elastic, volume-conserving model, this will produce an out-of-plane contraction of their lattice parameters with respect to STO of ≈1.8% for LSMO and 6% for LCO (a_{LCO} = 3.826 Å; a_{LSMO} = 3.881 Å, in a pseudocubic setting).

Geometric phase analysis (GPA),[31] combined with high-angle annular dark-field (HAADF) images from cross sectional lamellae of LSMO/LCO (see Figure S3 in the Supporting Information) show that the in-plane lattice parameter of both LCO and LSMO are well matched to the substrate. However, though the out-of-plane lattice parameter of LSMO presents an average contraction of ≈1.2%, close to expected value, the out-of-plane lattice parameter of LCO layer contracts about ≈3.5%. The contraction in LCO is substantially smaller than expected. This could be a signature of oxygen nonstoichiometry in the film, as observed previously when grown on top of STO under similar in-plane strain.[28,32]

To confirm the role of total strain and lattice symmetry effect on the volume of LCO, a trilayer of LCO/LSMO/LCO with identical thicknesses of the LCO layers was grown and analyzed by HAADF imaging in STEM and GPA. The results are summarized in Figure 2. The intermediate layer of LSMO was grown thick enough (22 nm) to maintain its bulk-like rhombohedral structure, as shown in ref 33. The rhombohedral symmetry of our LSMO films was verified by the existence of half-order (1/2, 1/2, 3/2) Bragg reflections (see Figure S4 in the Supporting Information). The results confirm that three layers grow fully strained with respect to the substrate. It is also clearly observed that the out-of-plane contraction, and thus the final volume, of LCO is independent of whether it is grown on top of STO or LSMO. Therefore, it depends only on the in plane strain, not on the symmetry of the material underneath.

The magnetic properties of the bilayers LSMO/LCO and LCO/LSMO are shown in Figure 3. For LCO/LSMO, low field magnetization versus temperature experiments confirmed the existence of a magnetic transition at ≈85 K, as expected on strained films on top of STO substrate (Figure S5 in the Supporting Information). This bilayer shows a single-step $M(H)$ loop, with a saturation magnetization at low temperature of ≈2.4 μ_B/Mn, and a coercive field, H_C ≈ 140 Oe (Figure 3a). This H_C is much larger than H_C ≈ 25 Oe for pure LSMO (Figure S5 in the Supporting Information), which demonstrates

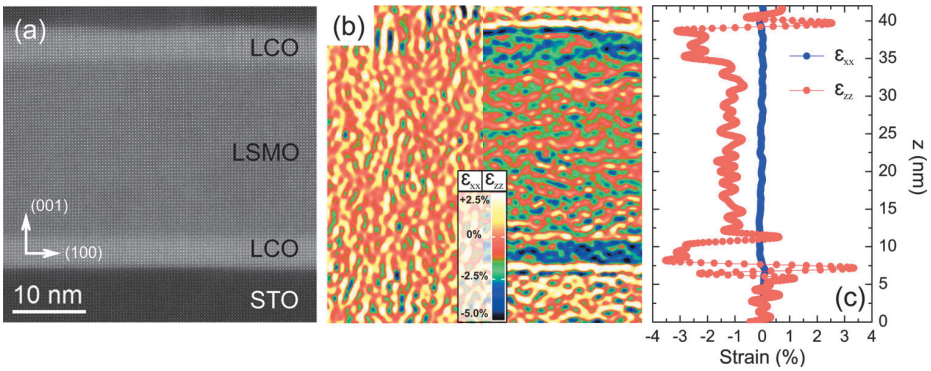

Figure 2. (a) HAADF-STEM image of the LCO/LSMO/LCO trilayer and (b) GPA analysis of that image showing the in-plane and out-of-plane deformation of the lattice parameter with respect to the STO substrate. (c) Line profiles of the in-plane and out-of-plane deformations integrated horizontally over 100 pixels. Note the same contraction in both layers of LCO (≈3.5%) when grown on top of LSMO or directly on STO.

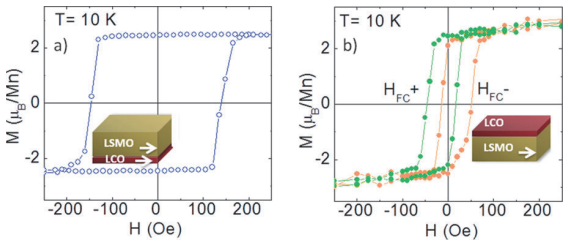

Figure 3. Magnetic hysteresis loop for the LCO/LSMO (a) and LSMO/LCO (b) bilayers, measured at 10 K. The $M(H)$ curve in the latter case moves to either + or − fields, depending on the sign of the applied field during cooling, due to exchange bias.

that the magnetization of LCO and LSMO are coupled through the interface and rotate simultaneously with H.

Surprisingly, the situation is completely different for the reverse configuration: LSMO/LCO. In this case, the $M(H)$ curve is similar to that of isolated LSMO, with a $H_C \approx 20$ Oe, confirming the suppression of ferromagnetism in LCO grown on top of rhombohedral LSMO. An exchange bias with $H_E \sim 17$ Oe is observed in this case (Figure 3b), most probably due to an antiferromagnetic Mn−O−Co superexchange coupling across the LSMO/LCO interface.

Therefore, our results demonstrate that FM is suppressed in the films of LCO grown on LSMO, although the unit cell volume (the total lattice deformation) of the LCO films is absolutely similar when grown directly on cubic STO or on top of a buffer layer of rhombohedral LSMO at STO (see GPA analysis in Figure 2).

This is a confirmation that it is the symmetry of the lattice underneath (not just the total strain) that plays the main role in the appearance of ferromagnetism in strained thin films of LCO. Accommodation of lattice strain and symmetry-mismatch changes the rotation pattern of CoO_6 octahedra in LCO with respect to bulk. Epitaxial matching to cubic STO (*Pm*-3m, #221, $a^0b^0c^0$) requires a distortion of the octahedral rotations in LCO with respect to bulk $R\bar{3}c$ (number 167, $a^-a^-a^-$). This changes the Co−O distance and the spin-state of Co^{3+}, as recently suggested.[29] On the other hand, the same rotation pattern is observed in rhombohedral LSMO, and therefore, a perfect symmetry matching occurs at the interface between these two oxides, leaving the Co−O covalency in LCO mostly unaffected.

Once we have confirmed that the FM of LCO can be maintained down to 3−4 nm under proper choice of the crystal underneath, we attempted the design of a multilayer heterostructrure in which an independent reversal of FMI-LCO and half-metal ferromagnet LSMO is achieved. This is a first step to probe the suitability of FMI-LCO as a spin-filter tunneling barrier.

In order to achieve this goal, a thin layer of STO was grown between the bottom film of LSMO and the top layer of LCO. To keep the total thickness of the insulating barrier constant, ≈1 nm of STO and ≈2.5 nm of LCO were grown on top of ≈20 nm of LSMO (Figure 4a). In this configuration, the STO barrier plays a dual role of maintaining the necessary distortion to produce FM behavior in the top LCO layer, and of decoupling the magnetization of LCO and LSMO. As shown in Figure 4, an STO layer ≈1 nm thick is enough to accomplish

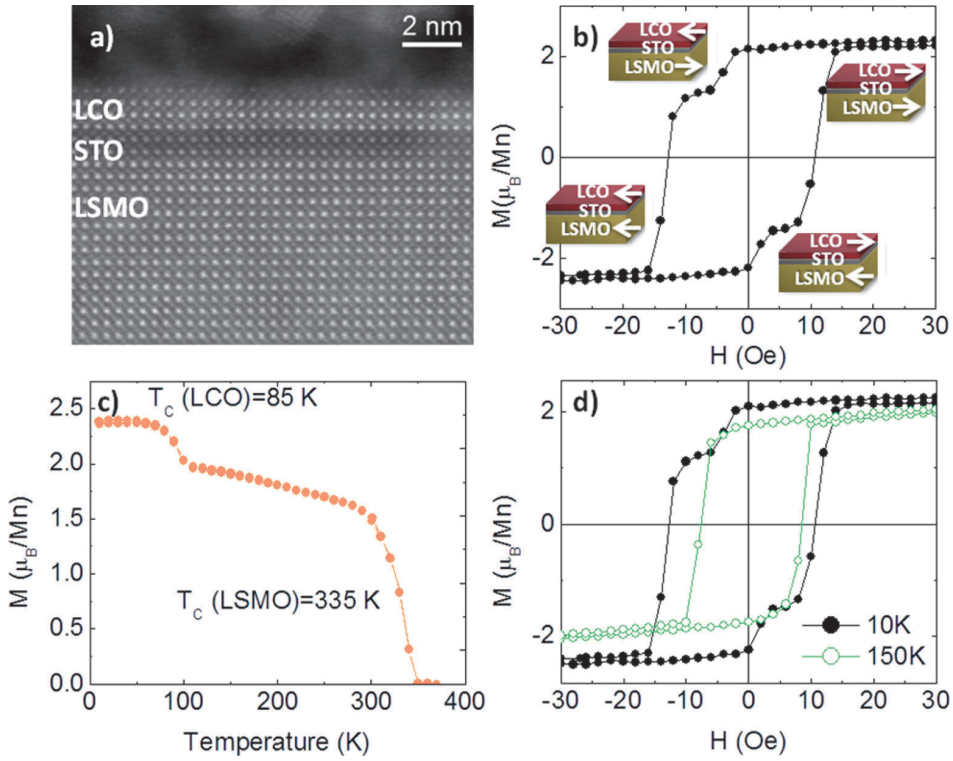

Figure 4. (a) HAADF-STEM image of the trilayer LSMO/STO/LCO sample. The thickness of the top LCO layer is slightly reduced from the as-deposited film, due to surface damage during preparation of the lamella. (b) Magnetic hysteresis loop of the sample at 10 K. (c) Magnetization versus temperature at low external field (8 Oe). (d) Comparison of the magnetic loops measured at 10 and 150 K. The two-step $M(H)$ curve is only observed below T_c of LCO (85 K). The loop measured at 150 K is similar to the loop of pure LSMO.

these objectives. This figure shows the two-step behavior in the hysteresis loop at 10 K, corresponding to the independent reversal of the magnetization of the LCO and LSMO layer. The variation in the magnetization at the step corresponds to ≈0.8 μ_B/Co, which is roughly the expected value for LCO.[28]

To demonstrate that this behavior is indeed reflecting the independent switching of the magnetization in both layers, we have measured the magnetization as a function of the temperature and the hysteresis loop at different temperatures. As shown in Figure 4c, two transitions are visible in the $M(T)$ curve, at 85 K from the LCO layer, and at 335 K, from the LSMO layer. Above T_C of LCO, the $M(H)$ curve of the trilayer recovers the single step behavior, at the time that the coercive field and the saturation magnetization decreases to the expected value for an isolated LSMO film (Figure 4d). These two experiments confirm that the magnetization of the LCO and LSMO layers rotate independently of each other. We noted that in this configuration the coercive field of the LCO layer is very small, ≈10 Oe. Although an important decrease of H_C is observed when thickness decreases (Figure S4 in the Supporting Information), this value seems too small even taken into account this possibility. Therefore, we are forced to conclude that the quality of the thin layer of LCO when deposited on top of ≈1 nm STO is not as good and free of defects as when deposited on the STO single-crystal substrate.

In summary, we have determined the conditions to grow ultrathin FMI layers of LCO. This was done by studying the role played by symmetry-mismatch (beyond the total strain) between LCO and the crystal underneath, to stabilize the FM interaction in the cobaltite. Finally, we have designed a multilayer heterostructure in which independent rotation of the magnetization of LCO and LSMO has been achieved. This is an important step forward for the development of spin-filtering tunneling devices based on FMI-LCO.

Experimental Section. Multilayers of LCO, LSMO and STO heterostructures were grown on TiO_2-terminated (001) STO by pulsed laser deposition (λ = 248 nm, KrF excimer laser). The ablation fluence, repetition rate and oxygen pressure were ≈0.9 J/cm^2, 5 Hz, and 200 mTorr, respectively. The LSMO and STO layers were grown at a substrate temperature of 800 °C, whereas the substrate temperature for LCO was optimized at 700 °C. X-ray characterization was performed in a PANalytical Empyrean diffractometer, using Cu Kα radiation. Scanning transmission electron microscopy (STEM) measurements were performed in a FEI Titan 60−300 operated at 300 kV and equipped with a high brightness Schottky field emission gun, a CETCOR probe aberration corrector from CEOS to provide a spatial resolution better than 1 Å in STEM mode, and a Gatan Imaging Filter 866 ERS for spectroscopic analysis. Z contrast imaging was carried out in high angle annular dark field (HAADF) with a probe convergence angle of 25 mrad and an inner collection angle of approximately 58 mrad. Additionally, HAADF imaging was combined with electron energy loss spectroscopy (EELS) to analyze chemically the heterostructures by STEM-EELS spectrum imaging. In this case, both the inner angle for the HAADF detector and the spectrometer collection angle were 60 mrad. Spectrum image (SI) has been performed with an energy dispersion of 0.5 eV and the dwell time around 0.04 s. The analyzed specimen is a lamella extracted from the sample by focused ion beam (FIB) milling in a FEI Helios Nanolab 600 using a 5 kV ion beam for the final thinning to reduce the surface amorphization layer. Magnetic measurements were performed using a Magnetic Property Measurement System (MPMS) from Quantum Design, with the magnetic field applied parallel to the film surface.

ACKNOWLEDGMENTS

This work was supported by the European Research Council (ERC StG-259082, 2DTHERMS, 312483-ESTEEM2), MINECO of Spain (MAT2013-44673-R and MAT2014-51982-C2-R) including FEDER funding, by Xunta de Galicia (2012-CP071 and 2015-CP081), and by the Aragón Regional Government through projects E26 and CTPP4/11. The microscopy works have been conducted in the Laboratorio de Microscopías Avanzadas (LMA) at the Instituto de Nanociencia de Aragón (INA)- Universidad de Zaragoza. Authors acknowledge the LMA-INA for offering access to their instruments and expertise. J. M. Vila-Fungueiriño from USC is acknowledged by assistance in X-ray measurements.

REFERENCES

(1) Moodera, J. S.; Santos, T. S.; Nagahama, T. *J. Phys.: Condens. Matter* **2007**, *19*, 165202−165225.
(2) Moodera, J. S.; Hao, X.; Gibson, G. A.; Meservey, R. *Phys. Rev. Lett.* **1988**, *61*, 637−640.
(3) Hao, X.; Moodera, J. S.; Meservey, R. *Phys. Rev. B: Condens. Matter Mater. Phys.* **1990**, *42*, 8235−8243.
(4) Moodera, J. S.; Meservey, R.; Hao, X. *Phys. Rev. Lett.* **1993**, *70*, 853−856.
(5) Santos, T. S.; Moodera, J. S. *Phys. Rev. B: Condens. Matter Mater. Phys.* **2004**, *69*, 241203−241207(R).
(6) Gajek, M.; Bibes, M.; Varela, M.; Herranz, G.; Fusil, S.; Bouzehouane, K.; Barthélémy, A.; Fert, A. *J. Appl. Phys.* **2006**, *99*, 08E504.
(7) Gajek, M.; Bibes, M.; Fusil, S.; Bouzehouane, K.; Fontcuberta, J.; Barthélémy, A.; Fert, A. *Nat. Mater.* **2007**, *6*, 296−302.
(8) Harada, T.; Ohkubo, I.; Lippmaa, M.; Sakurai, Y.; Matsumoto, Y.; Muto, S.; Koinuma, H.; Oshima, M. *Adv. Funct. Mater.* **2012**, *22*, 4471−4475.
(9) Lüders, U.; Barthélémy, A.; Bibes, M.; Bouzehouane, K.; Fusil, S.; Jacquet, E.; Contour, J.-P.; Bobo, J.-F.; Fontcuberta, J.; Fert, A. *Adv. Mater.* **2006**, *18*, 1733−1736.
(10) Caffrey, N. M.; Fritsch, D.; Archer, T.; Sanvito, S.; Ederer, C. *Phys. Rev. B: Condens. Matter Mater. Phys.* **2013**, *87*, 024419.
(11) Chapline, M. G.; Wang, S. X. *Phys. Rev. B: Condens. Matter Mater. Phys.* **2006**, *74*, 014418−014425.
(12) Ramos, A. V.; Guittet, M.-J.; Moussy, J.-B.; Mattana, R.; Deranlot, C.; Petroff, F.; Gatel, C. *Appl. Phys. Lett.* **2007**, *91*, 122107−122109.
(13) Ramos, A. V.; Santos, T. S.; Miao, G. X.; Guittet, M.-J.; Moussy, J.-B.; Moodera, J. S. *Phys. Rev. B: Condens. Matter Mater. Phys.* **2008**, *78*, 180402−180405(R).

(14) Sánchez, A. M.; Äkäslompolo, L.; Qin, Q. H.; van Dijken, S. *Cryst. Growth Des.* **2012**, *12*, 954−959.
(15) Goodenough, J. B. *Magnetism and the Chemical Bond*; John Wiley & Sons: New York, 1963.
(16) Fuchs, D.; Pinta, C.; Schwarz, T.; Schweiss, P.; Nagel, P.; Schuppler, S.; Schneider, R.; Merz, M.; Roth, G.; Löhneysen, H. v. *Phys. Rev. B: Condens. Matter Mater. Phys.* **2007**, *75*, 144402−144406.
(17) Fuchs, D.; Arac, E.; Pinta, C.; Schuppler, S.; Schneider, H.; Löhneysen, H. v. *Phys. Rev. B: Condens. Matter Mater. Phys.* **2008**, *77*, 014434−014441.
(18) Park, S.; Ryan, P.; Karapetrova, E.; Kim, J. W.; Ma, J. X.; Shi, J.; Freeland, J. W.; Wu, W. *Appl. Phys. Lett.* **2009**, *95*, 072508−072510.
(19) Sterbinsky, G. E.; Ryan, P. J.; Kim, J.-W.; Karapetrova, E.; Ma, J. X.; Shi, J.; Woicik, J. C. *Phys. Rev. B: Condens. Matter Mater. Phys.* **2012**, *85*, 020403−020407.
(20) Rivadulla, F.; Bi, Z.; Bauer, E.; Rivas-Murias, B.; Vila-Fungueiriño, J. M.; Jia, Q. X. *Chem. Mater.* **2013**, *25*, 55−58.
(21) Haverkort, M. W.; Hu, Z.; Cezar, J. C.; Burnus, T.; Hartmann, H.; Reuther, M.; Zobel, C.; Lorenz, T.; Tanaka, A.; Brookes, N. B.; Hsieh, H. H.; Lin, H.-J.; Chen, C. T.; Tjeng, L. H. *Phys. Rev. Lett.* **2006**, *97*, 176405−176408.
(22) Goodenough, J. B. Metallic Oxides, *Progress in Solid State Chemistry*, Vol. 5; Reiss, H., Ed.; Elsevier B.V.: Amsterdam, 1971.
(23) Choi, W. S.; Kwon, J.-H.; Jeen, H.; Hamann-Borrero, J. E.; Radi, A.; Macke, S.; Sutarto, R.; He, F.; Sawatzky, G. A.; Hinkov, V.; Kim, M.; Lee, H. N. *Nano Lett.* **2012**, *12*, 4966−4970.
(24) Hsu, H.; Blaha, P.; Wentzcovitch, R. M. *Phys. Rev. B: Condens. Matter Mater. Phys.* **2012**, *85*, 140404−140408.
(25) Kwon, J.-H.; Kwon, J.-H.; Choi, W. S.; Kwon, Y.-K.; Jung, R.; Zuo, J.-M.; Lee, H. N.; Kim, M. *Chem. Mater.* **2014**, *26*, 2496−2501.
(26) Freeland, J. W.; Ma, J. X.; Shi, J. *Appl. Phys. Lett.* **2008**, *93*, 212501−21503.
(27) Biškup, N.; Salafranca, J.; Mehta, V.; Oxley, M. P.; Suzuki, Y.; Pennycook, S. J.; Pantelides, S. T.; Varela, M. *Phys. Rev. Lett.* **2014**, *112*, 087202−087206.
(28) Mehta, V. V.; Biskup, N.; Jenkins, C.; Arenholz, E.; Varela, M.; Suzuki, Y. *Phys. Rev. B: Condens. Matter Mater. Phys.* **2015**, *91*, 144418−144430.
(29) Qiao, L.; Jang, J. H.; Singh, D. J.; Gai, Z.; Xiao, H.; Mehta, A.; Vasudevan, R. K.; Tselev, A.; Feng, Z.; Zhou, H.; Li, S.; Prellier, W.; Zu, X.; Liu, Z.; Borisevich, A.; Baddorf, A. P.; Biegalski, M. D. *Nano Lett.* **2015**, *15*, 4677−4684.
(30) Glazer, A. M. *Acta Crystallogr., Sect. B: Struct. Crystallogr. Cryst. Chem.* **1972**, *28*, 3384−3392.
(31) Hytch, M. J.; Snoeck, E.; Kilaas, R. *Ultramicroscopy* **1998**, *74*, 131−146.
(32) Klenov, D. O.; Donner, W.; Foran, B.; Stemmer, S. *Appl. Phys. Lett.* **2003**, *82*, 3427−3249.
(33) Sandiumenge, F.; Santiso, J.; Balcells, L.; Konstantinovic, Z.; Roqueta, J.; Pomar, A.; Espinós, J. P.; Martínez, B. *Phys. Rev. Lett.* **2013**, *110*, 107206−107210.